International Journal of Physics and Applications

E-ISSN: 2664-7583
P-ISSN: 2664-7575
IJOS 2021; 3(2): 14-21

www.physicsjournal.in
Received: 05-09-2021
Accepted: 11-10-2021

Kola Srimannarayana
Lecturer, Department of Physics, Government Degree College, Marripalem, Andhra Pradesh, India

Corresponding Author:
Kola Srimannarayana
Lecturer, Department of Physics, Government Degree College, Marripalem, Andhra Pradesh, India

Cerium substituted BCZT-ceramics synthesized through microwave assisted solid state reaction method

Kola Srimannarayana

DOI: https://doi.org/10.33545/26647575.2021.v3.i2a.94

Abstract
In this research article investigated and studies on Ce^{4+} substitution lead free prepared by microwave heating. XRD, SEM and FTIR techniques used for structural studies. Studied the crystallinity, particle density, micro strain and dislocation densities, lattice parameters by using irregular morphologies, according to the SEM study.

Keywords: BCZT-ceramics, solid state reaction, particle density, micro strain, dislocation densities

Introduction
The ferroelectric materials are extensively used in various practical applications in electrical electronics and computer industry [1-2]. The higher performance lead based ferroelectric materials were extensively used but these materials are hazardous to environment and humans [3-6]. Lead free ferroelectric perovskite $BaTiO_3$ was discovered [6] and it has ABO_3 symmetry. To enhance the the dielectric and ferroelectric properties of ABO_3 symmetry a lot of work has been done by substituting $ca^{2+}, Sr^{2+}, and\ Mg^{2+}$ at the A site and Sn^{2+} , Zr^{4+}, Mn^{3+} , $Co^{3+}, Fe^{3+},$ at the B site. Barium calcium Zirconium Titanate (BCZT), high piezoelectric coefficient ($d_{33} = 600pC/N$) and electromechanical coupling coefficient [7], an alternative to lead based ferroelectric materials. Many researchers are trying to synthesize new compositions by partially doping certain ratios of calcium by replacing the same ratio of barium and also by replacing titanium with zirconium for improving ferro and piezoelectric properties. In this work, the author substituted CeO_2 in BCZT and took the compositions of $Ba_{0.85}Ca_{0.15}Zr_{0.9-x}Ce_xTi_{0.1}O_3\ for$ x=0.005, 0.01, 0.015, 0.020. Microwave sintering was used for sintering. The structural properties were characterized by XRD, FTIR and SEM

Experimental Methods
The solid-state reaction technique was used to synthesize $Ba_{0.85}\ Ca_{0.15}\ Zr_{0.9-x}\ Ce_x\ Ti_{0.1}\ O_3\ (x = 0,0.005,0.010,0.010,0.015,0.020)$. Powdered forms of the anhydrous raw materials BaO, CaO, CeO_2, ZrO_2, and TiO_2 with 99.9% purity were consumed. Equation was used to weigh these materials based on their stoichiometric ratio.

$$0.85BaO + 0.15CaO + (0.9 - x)ZrO_2 + xCeO_2 + 0.1TiO_2 \rightarrow Ba_{0.85}Ca_{0.15}Zr_{0.9-x}Ce_xTi_{0.1}O_3$$

For homogeneity, the weighted raw components were pestle-ground for four hours in an agate mortar. For four hours, these Ce-doped powder samples were calcined at 1100 °C. To create a fine powder, the calcined samples were milled for thirty minutes. These powder samples were mixed with a few drops of polyvinyl alcohol (PVA) binders and processed again until the combination returned to its original dried, non-viscous state. Subsequently, a hydraulic press operating at a pressure of $5\ tons/cm^2$ was utilized to manufacture pellets with a diameter of roughly 10 mm and a thickness of 1.5 to 2 mm. The ready-made pellets were sintered for thirty minutes at 1500 °C in the microwave furnace.

In order to examine the structural and morphological characteristics, the sintered pellets were broken into pieces and once more ground into a fine powder using an agate mortar and pestle.
In order to examine the crystal structures, the powdered microwave sintered pellets were subjected to an x-ray diffraction method up to 2θ and 80 °C scans using a Bruker D8 advanced Diffractometer at 25 ºC with cuKα1 radiation (=1.54060 Å). Phase's formation was recognized by its JCPDS card number, 01-079-2265.

The d spacing d_{hkl} was determined from the following formula

$$d_{hkl} = \frac{\lambda}{2\sin\theta}$$

The lattice cost. (a_o) was calculated using the following formula

$$a_o = d_{hkl}\sqrt{h^2 + k^2 + l^2}$$

Where h, k, l are Miller indices
The Debye Scherrer's formula [8] is used calculate the crystallites sizes of the $Ba_{0.85}Ca_{0.15-x}Sr_xZr_{0.9}Ti_{0.1}O_3$

$$D_{110} = \frac{0.9\lambda}{\beta\cos\theta}$$

Where λ is the x-ray wavelength, θ is the Bragg angle and β =full width at half maximum (FWHM)
The sample was analyzed using the Williamson-Hall (W-H) method in order to distinguish between strain-and size-induced broadenings. The Williamson-Hall approach

$$\beta^2 = \beta_{size}^2 + \beta_{strain}^2$$

$$\frac{\beta\cos\theta}{\lambda} = \frac{1}{D} + \frac{4\epsilon\sin\theta}{\lambda}$$

Where β = FWHM size, β_{size} = crystallite size FWHM, β_{strain} = micro strain by the effect of considering FWHM, Equation (2) is used to make a plot between $\frac{\beta cos\,\delta}{\lambda}$ (along the y-axis) and $sin\,\delta/\lambda$ (along the x-axis). The microstrain is given by the slope of the plot, and the crystallinity (D) is obtained by taking the reciprocal of the y-intercept.
The Nelson-Riley extrapolation method is used to calculate exact lattice parameters. This Nelson-Riley function is given by

$$F(\theta) = \frac{1}{2}\left[\left(\frac{\cos^2\theta}{\sin\theta}\right) + \left(\frac{\cos^2\theta}{\theta}\right)\right]$$

The real lattice parameter of the sample is given by the y-intercept of the plot formed between the change of lattice parameter a_o (along the y-axis) and F(θ) (along the x-axis).
The relative densities of the particles were measured by Archimedes' buoyancy principle and the relative density was calculated by the formula

$$d = \frac{W_a}{W_a - W_w}$$

Where W_a = samples weight in air, W_w = samples weight in water
The X-ray diffraction densities for various concentrations of Ce were calculated by Smith and Wijn [9] relation as follows

$$d_x = \frac{ZM}{Na_o^3}$$

Here d_x = molecular density, *M* = Molecular weight, *N* = Avagadro's Number and Z = number of molecules / unit cell. (One for perovskite) [10]

The Bulk density of the molecule was calculated by the following relation [11]

$$d = \frac{m}{V} = \frac{m}{\pi r^2 t}$$

Where m = mass (gm), v = volume(c.c), r = radius (cm), t = thickness of the pellet of the sample (cm)

The percentage of porosity was calculated from the relation [12]

Percentage of porosity $P\,\% = \left[1 - \frac{d}{d_x}\right] \times 100$

The dislocation density was calculated from the relation [13]

$$\delta = \frac{1}{D^2}$$

Here D is the crystallinity size obtained from W-H and Scherrer method

To examine the microstructures, the Ce doped ceramic sample pieces were put under a scanning electron microscope using an energy dispersive X-ray spectroscope (Jeol 6390LA/OXFORD XMX N) with an operating voltage of 20,000V and a magnification of X10000. Using the image J program, the porosity of the crystal and grain size were also determined from the SEM pictures.

Using Fourier-transformed infrared spectroscopy (FTIR-Thermo Nicolet IS50 4000 cm^{-1} to 100 cm^{-1}), the sintered pellet fragments were examined. In order to observe the alteration of chemical bonds by detecting vibrational modes, it is also utilized to collect high-resolution spectral data in the wave number range between 4000 cm^{-1} and 100 cm^{-1} using the KBr pelletization process. Using an FTIR spectrometer

3. Results and Discussion

3.1. XRD studies

Lead-free ceramics in powder form $Ba_{0.85}\ Ca_{0.15}\ Zr_{0.9-x}$ To investigate the structural characteristics at room temperature, $Ce_x\ Ti_{0.1}\ O_3$ with x=0, 0.005, 0.010, 0.015, and 0.020 were subjected to x-ray diffraction in the 2θ range between 20° and 80°. With an increase in Ce^{4+} concentration, the peaks somewhat migrated towards the lower 2θ angles. These diffraction patterns show a perovskite structure devoid of any secondary phase, indicating that Zr^{+4} ion and Ce^{4+} filled the Ti-sites while Ba-sites were occupied by Ca^{2+}. About 2θ = 45^0, no splitting is seen at (200).According to their intensity ratio, cubic symmetry was present in every sample. The XRD structure's peak displacement is depicted in Figure1.and is attributed to changes in the lattice characteristics that result from adding Zr replacement.

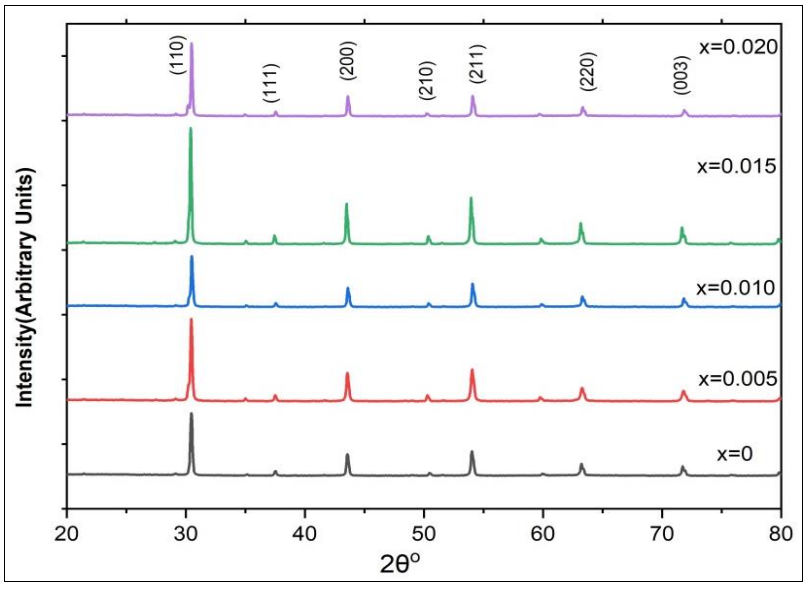

Fig 1: X-ray diffraction pattern of $Ba_{0.85}Ca_{0.15}Zr_{0.9-x}Ce_xTi_{0.1}O_3$

The positions of the peaks did not significantly change when Ce was doped into BCZT. The XRD pattern's distinct and sharp peaks show the formation of pure crystalline materials.

Table 1 illustrates how the lattice parameter (a_o) varies somewhat with Ce^{4+} concentration. This explains why average grain size reduced as Ce doping level increased. The reason for this is that Ce^{4+} has a bigger ionic radius than Ca^{2+}, therefore it replaces the Zr^{4+} ion. At x=0.005, it was found that the X-ray density was decreasing. Later, when the concentration of Ce grew, the densities climbed and reached their maximum at x=0.020. This is a result of higher density and higher atomic number Zr^{4+} ions replacing lower density and lower atomic weight Zr^{4+} ions. $Ba_{0.85}\ Ca_{0.15}\ Zr_{0.9-x}\ Ce_x\ TiO_3$ had experimental densities that were marginally lower than theoretical densities.

Table 1: The various parameters of $Ba_{0.85}Ca_{0.15}Zr_{0.9-x}Ce_xTi_{0.1}O_3$ for x=0, 0.005, 0.010, 0.015, 0.020

x	$x=0$	$x=0.005$	$x=0.010$	$x=0.015$	$x=0.020$
Theoretical densities(gm/cc)	6.05	5.98	6.08	6.05	6.09
Exp, density (gm/cc)	4.75	5.39	5.63	5.61	5.65
Relative density	5.87	5.72	5.72	5.77	5.76
$a_0\ (A^0)$	4.13	4.15	4.12	4.14	4.13
$a_0\ (A^0)$(Nelson Filer plot)	4.11	4.12	4.11	4.12	4.11
Porosity (%)	21.53	9.79	7.44	7.31	7.223

The Williamson Hall Plots of all samples were shown in Fig 2 (a-e). These plots indicate the anisotropic nature of samples [14] The crystallite sizes were measured between 6.8912$A^o$to and 29.4A^o similar to the values obtained from the Scherrer's method.

The unit cell either contracts or expands when a foreign element is doped into another element. The contraction of the atomic cell is caused by the greater atomic radius of Ce^{4+} (0.181 nm) compared to Zr^{4+} (0.160 nm). The micro strain was found to be reduced at x=0.5 based on the W-H plots.The negative microstrain values found in the Williamson-Hall plot served as an indicator of this.

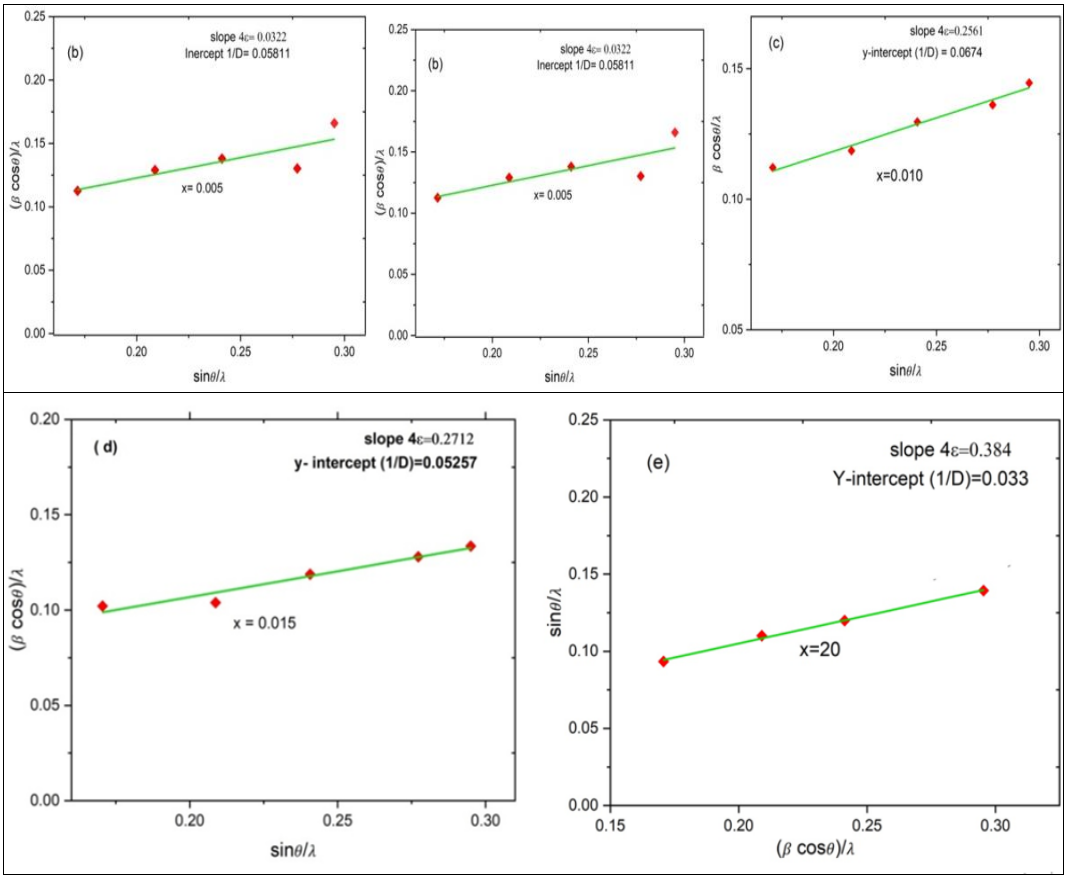

Fig 2: W-H plots of $Ba_{0.85}Ca_{0.15}Zr_{0.9-x}Ce_xTi_{0.1}O_3$ for x=0, 0.005, 0.010, 0.015, 0.020

The crystallinity D determines the dislocation density (δ), where a decrease in dislocation density signifies an increase in the crystal's crystallinity. The dislocation densities were computed using the W-H method, as seen in Figure 2.While the dislocation factor likewise decreases linearly with increasing Ce concentration, crystallinity grows linearly with increasing Ce concentration. This lowest dislocation factor shows that Ce^{4+} successfully replaced Zr^{4+} in the samples.

The exact lattice parameters of $Ba_{0.85}\ Ca_{0.15}\ Zr_{0.9-x}\ Ce_x\ Ti_{0.1}\ O_3$ were determined using the Nelson-Riley extrapolation method (N-R method). The N-R plot slopes in Fig. 2 provide the precise lattice characteristics of the samples. The values obtained from equation (1) nearly match these lattice characteristics.

Table 2: Structural parameters calculated from Williamson-Hall plots

for $Ba_{0.85}Ca_{0.15}Zr_{0.9-x}Ce_xTi_{0.1}O_3$ for x=0, 0.005, 0.010, 0.015, 0.020			
Ce concentration		**Structural parameters**	
X	**D** (A^o)	ϵ	$\delta\ (A^{o^{-2}})$
0	6.72	0.0210	0.020
0.005	17.01	0.0082	0.0034
0.01	14.29	0.0170	0.005
0.015	18.8	0.0682	0.004
0.02	29.90	0.0961	0.002

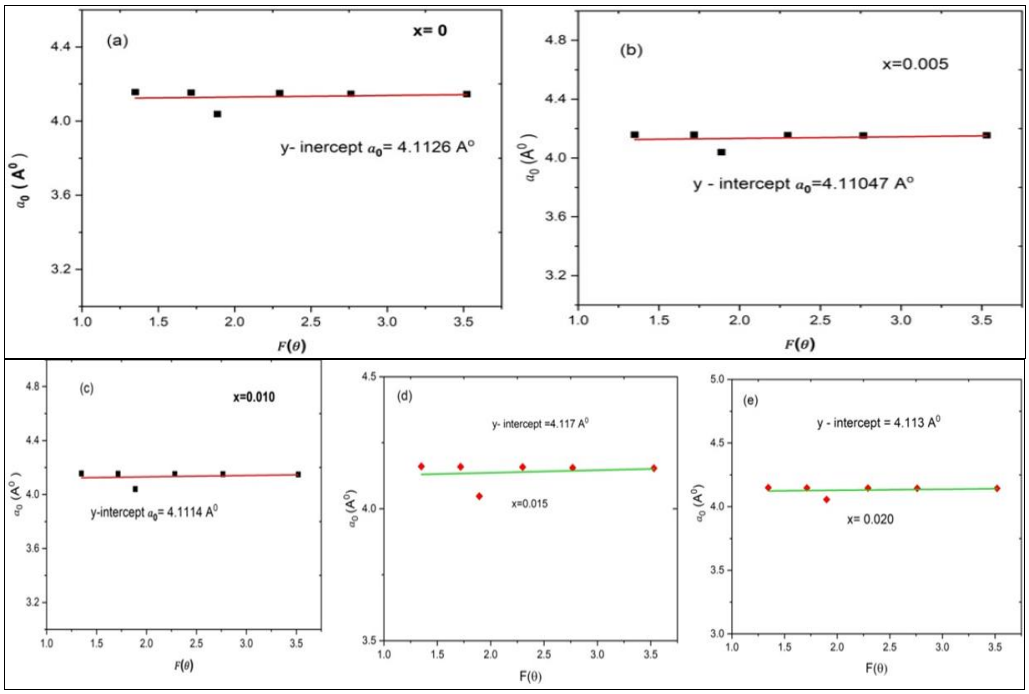

Fig 3: Nelson-Riley plots of $Ba_{0.85}Ca_{0.15}Zr_{0.9-x}Ce_xTi_{0.1}O_3$ represent the variation of F(θ) with lattice const (a_0) for x=0, 0.005, 0.010,0.015, 0.020

The fluctuation in Ce concentration was reflected in the variation of the lattice parameter a_o. The concentration of Ce has caused a_o to decrease approximately linearly as the percentage of Ce has climbed from x=0 to x=0.020.It was depicted in Figure 4.This is because Ce^{4+} and Ti^{4+} form a strong chemical bond that substitutes Zr^{4+}ions in $Ba_{0.85}\ Ca_{0.15}\ Zr_{0.9-x}.Ce_x\ Ti_{0.1}\ O_3$

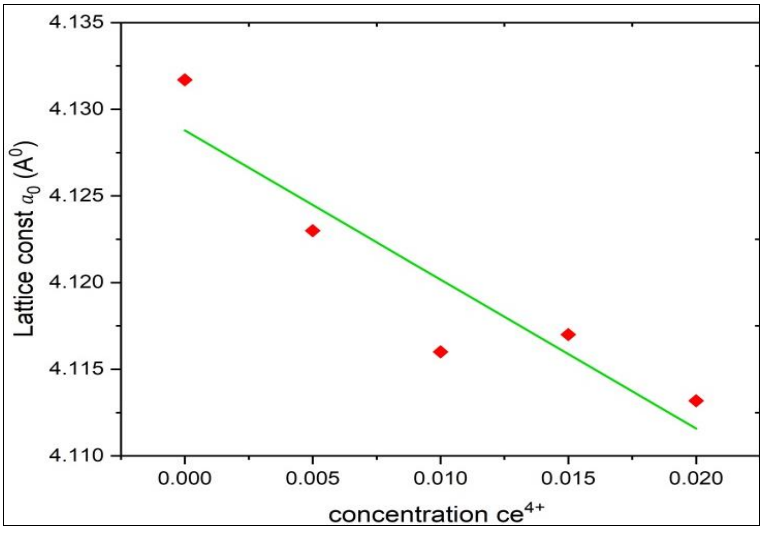

Fig 4: The fluctuation of a_o with the concentration of Ce for $Ba_{0.85}Ca_{0.15}Zr_{0.9-x}Ce_xTi_{0.1}O_3$ is plotted in.

3.2 SEM Analysis

The image software is used for analyzing SEM images of $Ba_{0.85}Ca_{0.15}Zr_{0.9-x}Ce_xTi_{0.1}O_3$. The average particle size and surface porosity were determined using SEM images, and it was observed that the surface porosity varied in accordance with Ce. The SEM images show that the surface porosity values are consistent with the porosity calculated from the XRD data, indicating a uniform distribution of pores within the crystal. The particles in all samples range in size from 1.45μ to 1.82μrs, with an irregular shape. The average size increases with Ce concentration. See Table 3 for details and Figure 5 for images.

Table 3: Physical parameters calculated from SEM for $Ba_{0.85}Ca_{0.15}Zr_{0.9-x}Ce_xTi_{0.1}O_3$

Concentration of Ce	**X=0**	**X=0.005**	**X=0.010**	**X=0.015**	**X=0.020**
Average size(μm)	1.45	1.61	2.25	1.52	1.82
Surface porosity	21.7	8.1	7.2	7.1	6.90

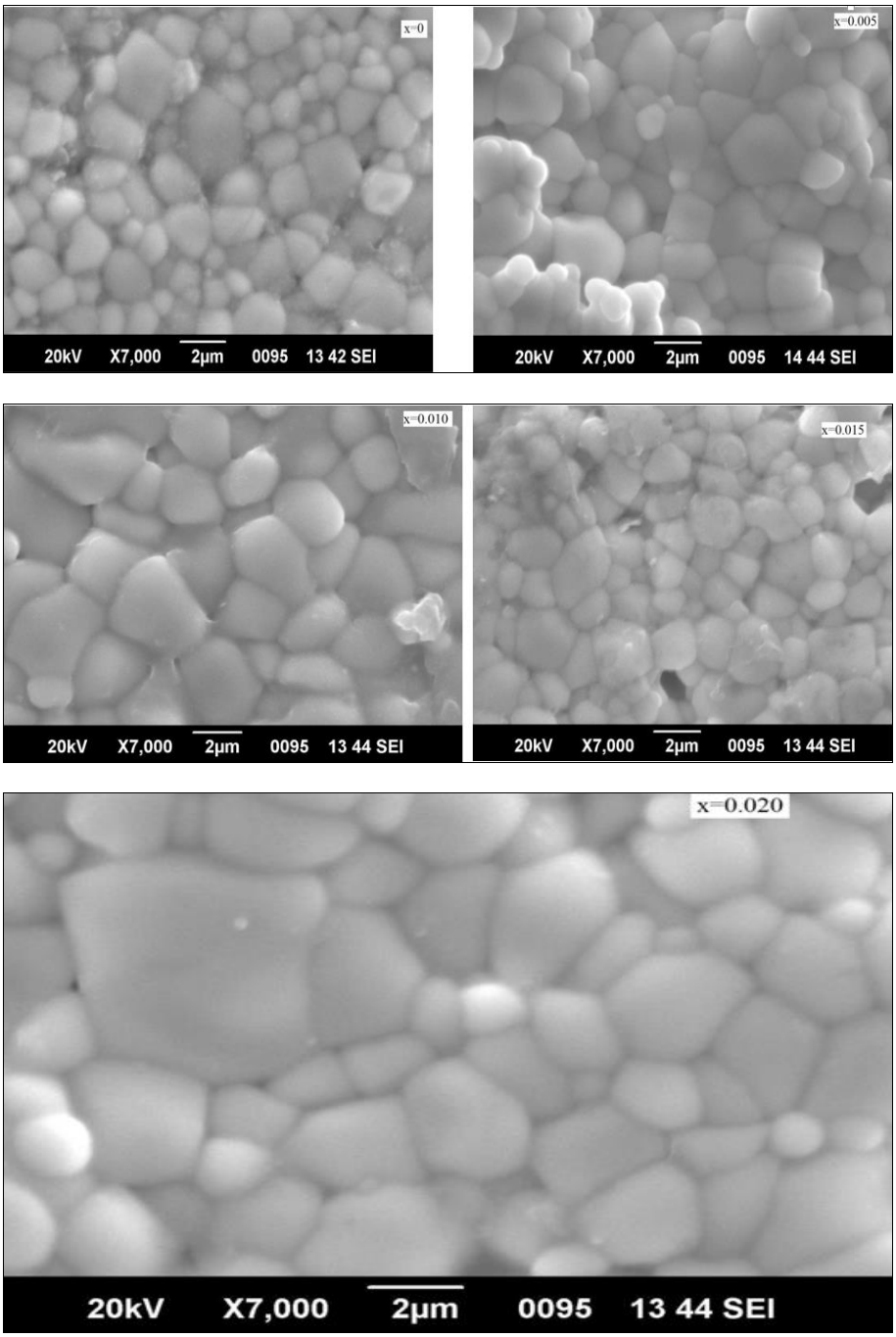

Fig 5: SEM images of $Ba_{0.85}Ca_{0.15}Zr_{0.9-x}Ce_xTi_{0.1}O_3$ for x=0, 0.005, 0.010, 0.015, 0.02

3.3 FTIR Analysis

In order to comprehend the diversity of chemical bonds in the crystal, the vibrational modes are measured using the FTIR technique. The molecular vibration determines where the FTIR absorption peak is located. The wave numbers of the metal oxide

bonds Ca-O, Ce-O, Zr-O, Ba-O, and Ti-O fall between $500cm^{-1}\ and\ 700cm^{-1}$. FTIR spectra of samples are displayed in Figure 6. A comparable $BaTiO_3$ pattern is projected to the peaks of all the samples of $Ba_{0.85}\ Ca_{0.15}\ Zr_{0.9-x}\ Ce_x\ Ti_{0.1}\ O_3$. The peak shifts from $554\ cm^{-1}$ toward a higher wave number of $557.84\ cm^{-1}$ as the concentration of Ce^{4+} increases. This results from the Ti-O bond being stretched when the Ce^{4+} ion is present. The obtained absorption peaks' shifting is seen in the FTIR spectrum.

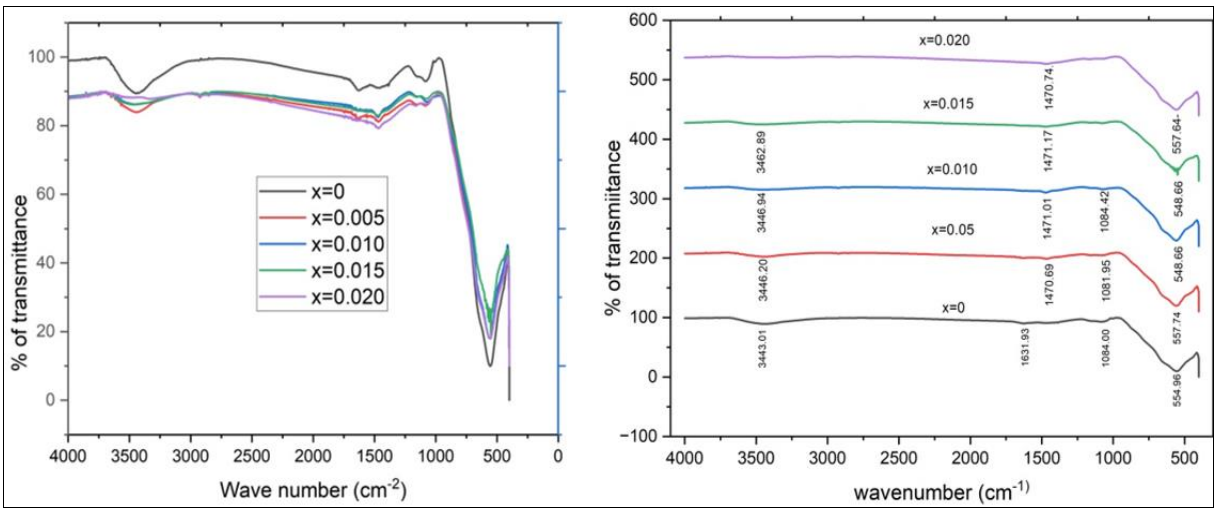

Fig 6: FTIR plot of $Ba_{0.85}Ca_{0.15}Zr_{0.9-x}Ce_xTi_{0.1}O_3$ for x=0, 0.005, 0.010, 0.015, 0.020

4. Conclusion

Solid state reaction was used to prepare the Ce^{4+} substitution of $Ba\_0.85\ Ca\_0.15\ Zr\_(0.9-x)\ Ce\_x\ Ti\_0.1\ O\_3$ ceramic particles. As the concentration of Ce^{4+} ions grew, the average size of the particles increased while the lattice characteristics, densities, and porosity dropped. Broad peaks are visible in the FTIR analysis for all Ce^{4+} values.The particles have irregular forms, according to SEM examination, and the surface porosity determined from the SEM pictures matched the xrd.

5. References

1. Zhou Z, Tang H, Sodano HA. Adv. Mater. 2014;26:7547.
2. Koruza J, Bell AJ, Frömling T, Webber KG, Wang K, Rödel J. J. Mater. 2018;4:13.
3. Saito Y, Takao H, Tani T, Nonoyama T, Takatori K, Homma T, *et al*. Lead-free piezoceramics. Nature. 2004;432:84.
4. Rödel J, Jo W, Seifert KTP, Anton EM, Granzow T, Damjanovic D. Perspective on the Development of Lead-free Piezoceramics. J. Am. Ceram. Soc. 2009;92(6):1153.
5. Xiao DQ, Wu JG, Wu L, Zhu JG, Yu P, Lin DM, *et al*. Investigation on the composition design and properties study of perovskite leadfree piezoelectric ceramics. J. Mater. Sci. 2009;44:5408.
6. Chen H, Yang C, Fu C, Shi J, Zhang J, Leng W. Microstructure and dielectric Properties of BaZrxTi1-xO3. J. Mater. Sci.: Mater. Electron. 2008;19(4):379-382.
7. Liu W, Ren X. Large piezoelectric effect in Pb-free ceramics. Phys. Rev. Lett. 2009;103(25):257602.
8. Anupama M, Rudraswamy B, Dhananjaya N. Investigation on impedance response and dielectric relaxation of Ni-Zn ferrites prepared by self-combustion technique. J. Alloys Compd. 2017;706:554-561.
9. Verma V, Gairola SP, Mathpal MC, Annapoorni S, Kotnala RK. Magnetic and electrical properties of manganese and cadmium co-substituted lithium ferrite. J. Alloys Compd. 2009;481:872-876.
10. Verma V, Kotnala RK, Pandey V, Kothari PC, Radhapiyari L, Mathur BS. The effect on dielectric losses in lithium ferrite by cerium substitution. J. Alloys Compd. 2008;466:404-407.
11. Batoo KM, Kumar G, Yang Y, Al-Douri Y, Singh M, Jotania RB, *et al*. Structural, morphological and electrical properties of Cd2+ doped MgFe2-xO4 ferrite nanoparticles. J. Alloys Compd. 2017;726:179-186.